

Quark-gluon vertex from the Landau gauge Curci-Ferrari model

Marcela Peláez^{a,b}, Matthieu Tissier^a, and Nicolás Wschebor^b

^a*LPTMC, Laboratoire de Physique Théorique de la Matière Condensée,
CNRS UMR 7600, Université Pierre et Marie Curie,
boîte 121, 4 place Jussieu, 75252 Paris Cedex 05, France.*

^b*Instituto de Física, Facultad de Ingeniería, Universidad de la República,
J. H. y Reissig 565, 11000 Montevideo, Uruguay.*

(Dated: March 17, 2022)

We investigate the quark-gluon three-point correlation function within a one-loop computation performed in the Curci-Ferrari massive extension of the Faddeev-Popov gauge-fixed action. The mass term is used as a minimal way for taking into account the influence of the Gribov ambiguity. Our results, with renormalization-group improvement, are compared with lattice data. We show that the comparison is in general very satisfactory for the functions which are compatible with chiral symmetry, except for one. We argue that this may be due to large systematic errors when extracting this function from lattice simulations. The quantities which break chiral symmetry are more sensitive to the details of the renormalization scheme. We however manage to reproduce some of them with good precision. The chosen parameters allow to simultaneously fit the quark mass function coming from the quark propagator with a reasonable agreement.

PACS numbers: 12.38.-t, 12.38.Aw, 12.38.Bx, 11.10.Kk
Keywords:

I. INTRODUCTION

The precise shape of the quark-gluon vertex plays an essential role in the understanding of many important properties of the infrared behavior of QCD [1–3]. This vertex is in particular fundamental in the analysis of the origin of dynamical chiral symmetry breaking in the context of truncated Dyson-Schwinger (DS) equations. Indeed, the DS equation for the quark self-energy requires the knowledge of this vertex, together with the gluon two-point vertex function. Even if this kind of object depends on the gauge-fixing, one expects that the gauge-invariant physical content of the theory is encoded on its behavior. For example, the meson spectrum can be studied by injecting such vertices and two-point functions in appropriate Bethe-Salpeter equations, see for example [4–10]. For these reasons, the determination of the quark-gluon vertex has been a topic of intensive work in the past. It has been first studied in the perturbative domain. A general parametrization based on its symmetries and a one-loop calculation of the abelian part in Feynman gauge was performed in [11]. Some years later, the complete one loop calculation in an arbitrary linear covariant gauge and in arbitrary dimension was performed in [12] (where previous partial results are reviewed also). More recently the complete 2-loop off-shell calculation has been performed in $d = 4$ [13]. These perturbative studies lead to a satisfactory description of this vertex at high momenta. However, the infrared sector, which is of direct interest for the understanding of chiral symmetry breaking, is not accessible to perturbation theory. To cope with problem, mainly two methods have been used: lattice simulations and DS equations.

In both of these approaches, the most convenient gauge is the Landau gauge. From the lattice simulation side,

it is well-adapted because the gauge-fixing operation can be expressed in terms of an extremization, which can be implemented efficiently on the lattice. From the analytic side, this gauge has several advantages. First, it is a linear gauge condition that manifestly preserves Lorentz invariance. Second, among all linear covariant gauges, it is the only one that includes the symmetries of the Curci-Ferrari gauge [14–16]. This implies, in particular, the existence of some non-renormalization theorems, that simplify considerably the algebraic work [17–20]. Third, in this gauge, the gluon propagator is transverse. Consequently, only the vertices where the gluon lines are multiplied by transverse projectors contribute to the correlation functions. Accordingly, all consideration below will be done in this gauge fixing.

There have been many analysis of the infrared behavior of the quark-gluon vertex based in the study of truncated DS equations (for a review, see [3]; for more recent work on the subject, see [21–23]). In parallel the intermediate and infrared regime of the vertex has been studied by lattice simulations. Many tensorial components have been analyzed [24, 25] for some particular configuration of momenta. Moreover, for the tensorial component that is already present at bare level, which is expected to be “dominant”, more general configurations of momenta have been considered [26].

In continuum analytical approaches, the gauge fixing is generally implemented through the Faddeev-Popov construction, which is a perfectly valid procedure in the ultraviolet regime, where standard perturbation theory works well and where the Faddeev-Popov construction is well justified. However, for momenta smaller or of the order of 1 GeV (which is the typical energy scale of the strong interaction) this procedure is not fully justified. The standard lore is that it becomes inappropriate be-

cause the coupling grows and perturbation theory eventually becomes a very bad approximation scheme. This argument must be tempered because the real expansion parameter of QCD is of the order of $N\alpha_S/(4\pi)$ and because lattice simulations, at least in some renormalization schemes, indicate that this parameter remains moderate (see, for example [27]). Accordingly it is reasonable to believe that some sort of perturbation theory should give results that are in qualitative agreement with experiments or lattice simulations in that regime. There is, however, another reason why standard perturbation theory should become inappropriate in the infrared regime: the Faddeev-Popov procedure itself becomes questionable. This originates in the existence of Gribov copies [28] in covariant gauge-fixings of non-abelian gauge theories that are ignored in the Faddeev-Popov construction. These copies play no significant role in the ultraviolet regime but a systematic treatment of the associated ambiguity remains an open problem in the infrared.

The most developed procedure which aims at taking into account the effects of Gribov copies is probably the Gribov-Zwanziger (GZ) construction [29–32]. The purpose of this approach is to restrict the functional integral to the first Gribov region where the Faddeev-Popov operator is positive definite. Gribov showed that in this region there are no copies that are an infinitesimal transformation of one another. Unfortunately it was shown later that there are *finite* gauge transformations that preserve the Landau condition [33]. Consequently the GZ procedure does not remove all copies. Moreover, the implementation of the restriction of the functional integral to the first Gribov region is not completely justified from first principles.

Despite these difficulties, first studies of the GZ predicted that the gluon propagator would vanish at zero momentum, instead of diverging as in the bare theory. A similar behavior was found also as solutions of truncated DS equations [1, 34–36] and in Non-perturbative Renormalization Group (NPRG) calculations [37, 38] (for a general review on this formalism, see [39]). This kind of solution is called “scaling solution”. The suppression of the gluon propagator was rapidly confirmed by lattice simulations. However, when lattice simulations became more precise they showed that the gluon propagator in Landau gauge did not behave precisely as the “scaling solution” that DS had suggested, neither in quenched lattice simulations [40–46] nor in the presence of dynamical quarks [47, 48]. In fact, lattice simulations favored a gluon propagator which tends to a finite value at low momentum in $d = 4$. This massive behavior (sometimes called “decoupling” solution) gives a propagator which is suppressed with respect to the bare one but not as strongly as in the “scaling solution” of DS equations. In parallel such decoupling solutions were also obtained from DS and NPRG equations [38, 49–55], as well as in a “refined” version of the GZ construction [32].

Nowadays, all approaches finally converge toward a massive-like gluon propagator in Yang-Mills theory.

Moreover, in what concerns the ghost sector, there is also a consensus in favor of a massless behavior, with a slight enhancement at low energy but with the tree level power-law. Finally, we note that DS and NPRG equations favor a coupling constant bounded in the infrared at not too large values, see for instance [55].

All these observations led two of us to test whether a simple perturbative analysis where a massive gluon propagator was introduced at the bare level [14] could reproduce quantitatively the lattice data for several correlation functions. This lagrangian is invariant under a modified Becchi-Rouet-Stora-Tuytin (BRST) symmetry that ensures the renormalizability of the model [56–58]. However, because of the gluon mass, the associated transformation is not nilpotent. As a consequence, the textbook construction of a physical space based on the cohomology of the BRST charge does not apply. It must be stressed that this difficulty is common to all methods that go beyond the standard perturbative FP method. In particular, the standard definition of the physical space does not apply to the GZ model but even stronger, does not apply to the procedure implemented on Landau-gauge lattice simulations. In fact the standard perturbative definition based on the cohomology of the BRST operator includes in the physical space the transverse gluons. But this is not satisfactory for two reasons. First, on physical grounds, we know that gluons are confined and are not part of the physical spectrum. Second, if transverse gluons were in the physical space, the spectral density associated with their two-point function should be positive and lattice simulations clearly show positivity violations [59, 60].

All these considerations show that a proper definition of a physical space is an open and important problem. In this sense, the lack of a nilpotent BRST charge in the Curci-Ferrari should not prevent us from studying it in relation with the lattice simulations of correlation functions. It is an open question to know if one can define a physical space for the Curci-Ferrari model where all states would have a positive norm.

In the present article we exploit this massive extension of the Faddeev-Popov Lagrangian in order to study the quark-gluon vertex in Landau gauge. Our aim is twofold. First, we want to compare our findings with lattice simulation in order to have a further test of the ability of the Curci-Ferrari model to reproduce lattice simulations. As we show below, we are able to compute the *full* vertex at one loop in any dimension, for all tensorial structures and for any configuration of momenta. The comparison of this one loop result is in reasonable agreement with all available lattice data (in many cases the agreement is very good). In particular, we discuss in detail the results of a certain scalar function (λ_2 in the terminology of [24]) where a significant discrepancy has been observed between lattice and DS results [21, 22]. We discuss this discrepancy in detail giving a very simple explanation of its origin. Second (and more importantly) as explained before, this vertex is very important in various physi-

cal applications of DS and Bethe-Salpeter equations. We expect that the present result will be useful in future physical applications in these equations.

We want to stress here that, as it stands, the simple one-loop calculation presented in this article does not encode a spontaneous breaking of the chiral symmetry. However, the renormalization-group flow leads to a strong enhancement of the quark mass in the infrared, which mimicks, for all practical purposes, the behavior induced by this symmetry breaking. This is a key ingredient for reproducing the infrared behavior of the quark-gluon vertex.

The rest of the article is organized as follows. In Sec. II we describe in more details our model and shortly review the systematic comparison of one-loop computations with lattice data. We give some details on the one-loop calculations in Sec. III and finally present our results in Sec. IV.

II. THE MODEL

In this article, we pursue our systematic analysis of the correlation functions of QCD in the Landau gauge, in a scheme where perturbative calculations can be performed in a controlled way for all energies. As explained in the introduction we consider the (euclidean) Curci-Ferrari Lagrangian [14]:

$$\mathcal{L}_A = \frac{1}{4} F_{\mu\nu}^a F_{\mu\nu}^a + \partial_\mu \bar{c}^a (D_\mu c)^a + i h^a \partial_\mu A_\mu^a + \frac{m^2}{2} A_\mu^a A_\mu^a \quad (1)$$

where A_μ^a is the gauge field, c^a and \bar{c}^a are ghost and antighost fields, h^a is a Lagrange multiplier that enforces the Landau gauge condition $\partial_\mu A_\mu^a = 0$, g is the coupling constant and

$$F_{\mu\nu}^a = \partial_\mu A_\nu^a - \partial_\nu A_\mu^a + g f^{abc} A_\mu^b A_\nu^c, \\ (D_\mu c)^a = \partial_\mu c^a + g f^{abc} A_\mu^b c^c.$$

It is important to recall that mass is introduced at the level of the gauge-fixed action. As a consequence, the bare propagators decrease at large momenta as $1/p^2$ and the mass induces a soft breaking of the BRST symmetry. As a consequence, all the ultraviolet properties of the standard Faddeev-Popov action are preserved to all orders in perturbation theory, in particular renormalizability and the behavior of correlation functions.

One of the main consequences of the mass term is that the low energy properties of the system are more regular than within the usual Faddeev-Popov approach. In particular, it is possible to find renormalization schemes in which the coupling constant remains finite down to the deep infrared [61], at odds with the findings of standard perturbation theory which presents a divergence of the coupling constant at some energy of the order of 1 GeV. The absence of such a Landau pole opens the way to

a consistent treatment of the low energy regime of the theory within perturbation theory.

The general idea was tested in [61, 62] where the quenched gluon and ghost propagators were computed at one-loop order. The comparison with lattice data is very satisfactory, with a discrepancy of at most 10% in the whole range of energy. The analysis of the 3-point correlation functions (three gluons and ghost-gluon) was performed under the same line of investigation in [63]. The comparison with lattice data is also very good although the lattice data are more noisy in this case.

More recently, we have considered the influence of dynamical quarks on the theory, which are governed by the Lagrangian:

$$\mathcal{L}_\psi = \sum_{i=1}^{N_f} \bar{\psi}_i (-\gamma_\mu D_\mu + M_i) \psi_i, \quad (2)$$

where γ_μ are euclidean Dirac matrices satisfying $\{\gamma_\mu, \gamma_\nu\} = 2\delta_{\mu,\nu}$, the flavor index i runs over the N_f quark flavors¹ and the covariant derivative of the quark field reads

$$D_\mu \psi = \partial_\mu \psi - ig A_\mu^a t^a \psi. \quad (3)$$

In [64] we have included the one-loop contribution of the quarks to the previously computed gluon propagator and have computed the quark propagator to the same order. Again, the gluon propagator compares very well with the lattice results.² The quark propagator can be decomposed in two independent structures in spinor indices, often called the mass (proportional to the identity in spinor indices) and field renormalization (proportional to a Dirac matrix). The one-loop results for the quark mass is in good agreement with the lattice data. In particular, it reproduces the strong enhancement at energies smaller than roughly 2 GeV, which is reminiscent of the chiral symmetry breaking³. However, we do not expect that the present simple one-loop calculation can break spontaneously the chiral symmetry. On the other hand, the field renormalization of the quark is not reproduced correctly, even at a qualitative level. This can be attributed to the fact that the one-loop contribution to this quantity is unusually small [64]. Indeed, when the gluon mass is set to zero, the field renormalization has no contribution at one loop but it does have contributions at two-loops, that, in consequence, become dominant.

¹ In this article, we mainly consider degenerate quark masses. In this case, the sum over flavors can be replaced by N_f .

² Note that there is no direct influence of the quarks to the ghost propagator at one-loop. However, the presence of the dynamic quarks modify the β functions, which gives an indirect effect on the ghost propagator. Again, the comparison of the ghost propagator with lattice data is very satisfactory.

³ A similar behavior can be seen in the present study in the quenched approximation, see Fig 4 below.

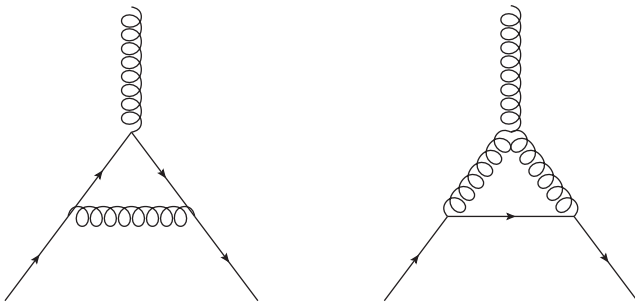


FIG. 1: One-loop Feynman diagrams for the quark-gluon vertex.

This model has also been used in another line of research in a recent series of articles: the extension of Yang-Mills theory at finite temperature was considered within the same framework with the goal of studying the deconfinement transition [65–67]. It was found that a simple one-loop calculation can reproduce the known phenomenology [second order transition for the SU(2) group and first order transition for SU(3)]. A next-to leading calculation in the SU(2) case leads to a quantitative agreement for the critical temperature.

III. ONE-LOOP CALCULATION

The determination of the quark-gluon vertex at one loop requires to compute the two diagrams depicted in Fig. 1. The result can be decomposed in twelve independent tensorial structures. We follow here the convention of [24] and express the quark-gluon vertex as

$$\Gamma_{\bar{\psi}\psi A_\mu^a}(p, r, k) = t^a \Gamma_\mu(p, r, k) \quad (4)$$

with

$$\Gamma_\mu(p, r, k) = -ig \left(\sum_{i=1}^4 \lambda_i L_{i\mu} + \sum_{i=1}^8 \tau_i T_{i\mu} \right). \quad (5)$$

We give in Table I the tensorial structures $L_{i\mu}$ and $T_{i\mu}$, together with some informations concerning the scalar functions λ_i and τ_i .

The calculations are performed by following the same procedure as described in [63, 64]. The Feynman rules are implemented in a Mathematica procedure and the integrals over momentum written in terms of the Passarino-Veltman integrals [68]:

$$A(m) = \int \frac{d^d q}{(2\pi)^d} \frac{1}{q^2 + m^2} \quad (6)$$

$$B_0(m_1, m_2) = \int \frac{d^d q}{(2\pi)^d} \frac{1}{[q^2 + m_1^2][(p+q)^2 + m_2^2]} \quad (7)$$

$$C_0(p_1, p_2, m_1, m_2, m_3) = \int \frac{d^d q}{(2\pi)^d} \frac{1}{[q^2 + m_1^2][(p_1+q)^2 + m_2^2][(p_1+p_2+q)^2 + m_3^2]} \quad (8)$$

Our expressions for the different scalar functions expressed in terms of these integrals are available in the supplemental material [69]. In actual calculations, it is convenient to use the Feynman trick to perform the integrals. In order to reduce the number of Feynman parameters, we use the identity:

$$\frac{1}{(q^2 + m_1^2)(q^2 + m_2^2)} = \frac{1}{m_1^2 - m_2^2} \left(\frac{1}{q^2 + m_2^2} - \frac{1}{q^2 + m_1^2} \right) \quad (9)$$

as many times as possible to reduce the number of propagators appearing in the diagrams. The price to pay is that there appears differences of masses in the denominator. For general momentum configurations, after performing the integrals over the internal momentum, we are left with a double integral over Feynman parameters. However, for integer space dimension and for some momentum configurations that are considered in next section, all integrals can be realized analytically. We thus obtain analytic expressions for the one-loop vertex for those configurations.

We have made several checks of our one-loop expressions. We have compared our results with those of [12] which were obtained in the limit of vanishing gluon mass. Our check consists in comparing numerically our results for vanishing gluon mass with those of [12]. This was done for several momentum configurations and we find a perfect agreement. Therefore, in the regime where the external momenta are large compared with the gluon mass, our results reproduce those of standard perturbation theory (including anomalous dimensions and all angular dependences). As a consequence, we do not study this regime further below.

Another check comes from the behavior of the coupling constants in the chiral limit (limit of vanishing quark mass). In this limit, we easily derive the Ward identity associated with the chiral symmetry:

$$\Gamma_\mu \gamma_5 + \gamma_5 \Gamma_\mu = 0, \quad (10)$$

where $\gamma_5 = \gamma_0 \gamma_1 \gamma_2 \gamma_3$. By using the anticommutation relations of Dirac Matrices, it is easy to check that, in the chiral limit, the structures $L_{3\mu}$, $L_{4\mu}$, $T_{1\mu}$, $T_{4\mu}$, $T_{5\mu}$ and $T_{7\mu}$ are not compatible with this Ward identity. We therefore conclude that the associated coupling constants must vanish in the chiral limit. We have explicitly verified that our one-loop expressions are compatible with this result.

We regularize the theory by using the Infrared-Safe (IS) scheme [61]. As usual, we introduce renormalized quantities, which are related to the bare ones by renormalization factors:

$$A_B = \sqrt{Z_A} A, \quad c_B = \sqrt{Z_c} c, \quad \bar{c}_B = \sqrt{Z_c} \bar{c},$$

$$\psi_B = \sqrt{Z_\psi} \psi, \quad \bar{\psi}_B = \sqrt{Z_\psi} \bar{\psi}, \quad (11)$$

$$g_B = Z_g g, \quad m_B^2 = Z_{m^2} m^2, \quad M_B = Z_M M. \quad (12)$$

| Coupl. cte. | Tensorial structure | Dim. of cte | Small M |
|-------------|---|---------------------|--------------------|
| λ_1 | $L_{1\mu} = \gamma_\mu$ | $(\text{GeV})^0$ | $\mathcal{O}(M^0)$ |
| λ_2 | $L_{2\mu} = -(\not{p} - \not{r})(p - r)_\mu$ | $(\text{GeV})^{-2}$ | $\mathcal{O}(M^0)$ |
| λ_3 | $L_{3\mu} = -i(p - r)_\mu$ | $(\text{GeV})^{-1}$ | $\mathcal{O}(M^1)$ |
| λ_4 | $L_{4\mu} = -i\sigma_{\mu\nu}(p - r)_\nu$ | $(\text{GeV})^{-1}$ | $\mathcal{O}(M^1)$ |
| τ_1 | $T_{1\mu} = i(k_\mu r_\nu k_\nu - r_\mu k^2)$ | $(\text{GeV})^{-3}$ | $\mathcal{O}(M^1)$ |
| τ_2 | $T_{2\mu} = (k_\mu r_\nu k_\nu - r_\mu k^2)(\not{p} - \not{r})$ | $(\text{GeV})^{-4}$ | $\mathcal{O}(M^0)$ |
| τ_3 | $T_{3\mu} = \not{k}k_\mu - k^2\gamma_\mu$ | $(\text{GeV})^{-2}$ | $\mathcal{O}(M^0)$ |
| τ_4 | $T_{4\mu} = -i[k^2\sigma_{\mu\nu}(p - r)_\nu - 2k_\mu\sigma_{\nu\lambda}r_\nu k_\lambda]$ | $(\text{GeV})^{-3}$ | $\mathcal{O}(M^1)$ |
| τ_5 | $T_{5\mu} = i\sigma_{\mu\nu}k_\nu$ | $(\text{GeV})^{-1}$ | $\mathcal{O}(M^1)$ |
| τ_6 | $T_{6\mu} = \not{k}(p - r)_\mu - k_\nu(p - r)_\nu\gamma_\mu$ | $(\text{GeV})^{-2}$ | $\mathcal{O}(M^0)$ |
| τ_7 | $T_{7\mu} = -\frac{1}{2}k_\lambda(p - r)_\lambda[(\not{p} - \not{r})\gamma_\mu - (p - r)_\mu] - i(p - r)_\mu\sigma_{\nu\lambda}r_\nu k_\lambda$ | $(\text{GeV})^{-3}$ | $\mathcal{O}(M^1)$ |
| τ_8 | $T_{8\mu} = -\gamma_\mu\sigma_{\nu\lambda}r_\nu k_\lambda + r_\mu\not{k} - \not{r}k_\mu$ | $(\text{GeV})^{-2}$ | $\mathcal{O}(M^0)$ |

TABLE I: We give the different tensorial structures on which the vertex was decomposed and the name of the associated (scalar) coupling constant. The last line describes the behavior of the coupling constant in the chiral limit.

The different renormalization factors are defined by imposing:

$$P_{\mu\nu}^\perp \Gamma_{A_\mu^a A_\nu^b}(p = \mu) = (d-1)\delta^{ab}(\mu^2 + m^2), \quad (13)$$

$$\Gamma_{c^a \bar{c}^b}(p = \mu) = \delta^{ab}\mu^2, \quad (14)$$

$$\Gamma_{\psi\bar{\psi}}(p = \mu) = M - i\not{p}|_{p^2=\mu^2}, \quad (15)$$

$$Z_A Z_c Z_{m^2} = 1, \quad (16)$$

$$Z_g \sqrt{Z_A} Z_c = 1. \quad (17)$$

The last two conditions are consequences of non-renormalization theorems which relate the divergent parts of the different renormalization factors [16–20]. Here, these relations are imposed also for the finite parts. The last renormalization condition corresponds to the Taylor scheme and is obtained by defining the coupling constant through the ghost-gluon vertex function with vanishing momentum for the external ghost. The condition (16) can not be expressed directly in terms of vertex (or correlation) functions. In particular, the mass parameter thus defined is not directly related to the value of the gluon propagator at vanishing momentum. Expressions for the renormalization factors can be found in [61, 64].

In the following, we use the renormalization-group improvement for the quark-gluon vertex. It is obtained by integrating the RG equation for the quark-gluon vertex function

$$\left[\mu \partial_\mu - \left(\frac{1}{2} \gamma_A + \gamma_\psi \right) + \beta_g \partial_g + \beta_{m^2} \partial_{m^2} + N_f \beta_M \partial_M \right] \Gamma_\mu = 0, \quad (18)$$

where

$$\beta_g(g, m^2, M) = \mu \frac{dg}{d\mu} \Big|_{g_0, m_0^2, M_0},$$

$$\beta_{m^2}(g, m^2, M) = \mu \frac{dm^2}{d\mu} \Big|_{g_0, m_0^2, M_0},$$

$$\gamma_A(g, m^2, M) = \mu \frac{d \log Z_A}{d\mu} \Big|_{g_0, m_0^2, M_0},$$

$$\gamma_c(g, m^2, M) = \mu \frac{d \log Z_c}{d\mu} \Big|_{g_0, m_0^2, M_0},$$

$$\beta_M(g, m^2, M) = \mu \frac{dM}{d\mu} \Big|_{g_0, m_0^2, M_0},$$

$$\gamma_\psi(g, m^2, M) = \mu \frac{d \log Z_\psi}{d\mu} \Big|_{g_0, m_0^2, M_0}.$$

By integrating Eq. (18) we relate the quark-gluon vertex at different scales through the equation:

$$\Gamma_\mu(\{p_i\}, \mu_0, g(\mu_0), m^2(\mu_0), M(\mu_0)) = \frac{\Gamma_\mu(\{p_i\}, \mu, g(\mu), m^2(\mu), M(\mu))}{\sqrt{z_A(\mu) z_\psi(\mu)}}. \quad (19)$$

Here $g(\mu)$, $m^2(\mu)$ and $M_i(\mu)$ are obtained by integrating the beta functions with initial conditions given at some scale μ_0 and:

$$\log z_A(\mu) = \int_{\mu_0}^{\mu} \frac{d\mu'}{\mu'} \gamma_A(g(\mu'), m^2(\mu'), M(\mu')),$$

$$\log z_c(\mu) = \int_{\mu_0}^{\mu} \frac{d\mu'}{\mu'} \gamma_c(g(\mu'), m^2(\mu'), M(\mu')),$$

$$\log z_\psi(\mu) = \int_{\mu_0}^{\mu} \frac{d\mu'}{\mu'} \gamma_\psi(g(\mu'), m^2(\mu'), M(\mu')).$$

Observe that the running quark mass appears explicitly in the previous expressions. This leads to a back-reaction of this running mass on the vertex functions. As a consequence, the mass takes very different values at $\mu = 0$ and $\mu = 1$ GeV. Even at a perturbative level, this is a large effect and, as discussed in the next section, is at the

origin of the enhancement of some scalar components of the vertex.

In the IS scheme, for the initial conditions of interest for comparing with the lattice data, the coupling constant does not present a Landau pole. In order to avoid large logarithms, we evaluate the right-hand-side of Eq. (19) with μ of the order of the external momenta when they are larger than the mass. In practice, we used $\mu = \sqrt{(p^2 + r^2 + k^2)/2 + m^2}$. It is important to stress that contrarily to what happens in the pure glue sector, there is a significative dependence on the scheme in the present calculation. In fact, it is important to choose the renormalization point at a scale that remain fixed when all momenta go to zero as done in [61].

In the following, we compare our results with lattice data which were obtained in the quenched approximation. Consequently, the beta functions for g and m as well as the anomalous dimensions for A and c are evaluated at $N_f = 0$. Therefore, the quark mass does not back-react on these quantities, but it does back-react on the vertex.

IV. RESULTS

The results presented in the previous section were obtained for an arbitrary momentum configuration and for all tensor structures. There have been lattice studies of the quark gluon vertex for general kinematics [26] for a particular tensorial structure in the quenched approximation. Our results are in general qualitative agreement with those of [26] at the level of precision of the data.

For some particular momentum configurations, lattice data were obtained with larger statistics and therefore smaller error bars. In the following, we concentrate on these configurations which give more stringent tests of the quality of our results. We perform a comparison with lattice data in three momentum configurations. The first one corresponds to configurations where the gluon has zero momentum with arbitrary momentum of the quark. In this configuration many tensorial structures were obtained in the quenched approximation [25] and we compare below our results for all available functions. The second configuration corresponds to equal momenta for the quark and antiquark (and, accordingly, gluon momentum equal to minus the double of them). Again, many tensorial structures were obtained in the quenched approximation for this configuration [25] and we study all of them below. On top of these two families of configurations, we consider a more general configuration with equal momentum in modulus of quarks and anti-quarks but for various possible angles between them (or, equivalently, different values of the modulus of the gluon momentum).

This configuration includes as particular cases the previous ones but for general angles only a single tensorial structure has been simulated [26] (also in the quenched approximation). For the comparison with the simulations, we focus on two values of modulus of the gluon momenta and also for the completely symmetric configuration where the incoming momentum of the gluon is equal in modulus to the quark and antiquark momenta. It must be pointed out that the employed data are more than ten years old. More recent data with improved lattice parameter could allow to perform a more precise test of our curves but they do not exist for the moment.

In the end of this section we finally discuss the effect of including dynamical quarks for the present vertex. Even if there are no simulations of this vertex in the unquenched case, there are some simulations of 2-point functions [73] that allows to fix the parameters and, in consequence, we are able to make a prediction of the behaviour of the quark-gluon vertex for the conditions that are present in those simulations. These could be compared to future unquenched simulations of the quark-gluon vertex.

A. Vanishing gluon momentum

Let us first consider the case of zero gluon momentum. In this case, the tensor structure simplifies to the following form

$$\Gamma_\mu(p, -p, 0) = -ig \left[\lambda_1(p^2)\gamma_\mu - 4\lambda_2(p^2)\not{p}p_\mu - 2i\lambda_3 p_\mu \right]. \quad (20)$$

Moreover, all integrals appearing in the vertex functions can be performed analytically. By introducing

$$\tilde{m} = \frac{me^{\gamma/2}}{\sqrt{4\pi}},$$

$$\mathbb{L}_1 = \log \left[\frac{(Y_1 - p^2)^2 - (M^2 - m^2)^2}{(Y_1 + p^2)^2 - (M^2 - m^2)^2} \right],$$

$$\mathbb{L}_2 = \log \left[\frac{(m^2 - M^2 - p^2)^2 - Y_1^2}{(m^2 - M^2 + p^2)^2 - Y_1^2} \right]$$

and

$$Y_1 = \sqrt{(m^2 - M^2 + p^2)^2 + 4M^2 p^2},$$

we obtain in $d = 4 - \epsilon$

$$\begin{aligned}
\lambda_1(p^2) = & 1 + \frac{3Ng^2}{32\pi^2} \left[\frac{1}{\epsilon} - \log(\tilde{m}) \right] \\
& + \frac{g^2}{192\pi^2 m^4 N p^4} \log\left(\frac{M}{m}\right) \left\{ -6m^8 (N^2 - 1) + m^6 [M^2 (10N^2 - 9) - (14N^2 + 3)p^2] \right. \\
& - 3m^4 [M^4 N^2 - 14M^2 p^2 + 3(N^2 + 2)p^4] + 3m^2 (M^6 - 7M^4 p^2 + 15M^2 p^4 - p^6) \\
& \left. - N^2 (M^2 + p^2)^4 \right\} - \frac{g^2}{192\pi^2 m^4 N p^4} \log\left(\frac{M^2 + p^2}{M^2}\right) (M^2 + p^2)^3 [N^2 (M^2 + p^2) - 3m^2] \\
& + \frac{g^2}{384\pi^2 m^4 N p^4 Y_1} \left\{ m^2 p^2 Y_1 [12m^4 (N^2 - 1) + m^2 M^2 (6 - 8N^2) + m^2 p^2 (19N^2 + 6)] \right. \\
& \left. - 6\mathbb{L}_2 (2m^2 - 5M^2 + p^2) (m^2 - M^2 + p^2) - 2N^2 (M^2 + p^2)^2 \right] \\
& + \mathbb{L}_1 \left[m^4 + 2m^2 (p^2 - M^2) + (M^2 + p^2)^2 \right] [6m^6 (N^2 - 1) + m^4 M^2 (3 - 4N^2) \\
& + m^4 (8N^2 - 3)p^2 - M^4 m^2 (N^2 - 3) + 6m^2 M^2 p^2 + m^2 (N^2 + 3)p^4 - N^2 (M^2 + p^2)^3] \left. \right\}, \quad (21)
\end{aligned}$$

$$\begin{aligned}
\lambda_2(p^2) = & \frac{g^2}{384\pi^2 m^2 N p^4} \left[12m^4 (N^2 - 1) - m^2 (4N^2 - 3) (2M^2 - p^2) - 2N^2 (M^2 + p^2)^2 \right] \\
& - \frac{g^2}{384\pi^2 m^4 N p^6} \log\left(\frac{M}{m}\right) \left\{ 12m^8 (N^2 - 1) - m^6 (10N^2 - 9) (2M^2 - p^2) + 6m^4 (M^4 N^2 + p^4) \right. \\
& + m^2 [-6M^6 - 9M^4 p^2 + 6M^2 (5N^2 - 1)p^4 + 9p^6] \\
& \left. + 2N^2 (M^8 + 4M^6 p^2 - 9M^4 p^4 + 19M^2 p^6 + p^8) \right\} \\
& - \frac{g^2}{384\pi^2 m^4 N p^6} \log\left(\frac{p^2}{M^2} + 1\right) (M^2 + p^2)^2 \left[m^2 (3p^2 - 6M^2) + 2N^2 (M^2 + p^2)^2 \right] \\
& + \frac{g^2}{768\pi^2 m^4 N p^8} \frac{\mathbb{L}_1}{Y_1} \left\{ 12m^{10} (N^2 - 1) p^2 + m^8 p^2 [M^2 (30 - 32N^2) + (22N^2 - 21)p^2] \right. \\
& + m^6 p^2 [2M^4 (13N^2 - 9) + 3M^2 (1 - 2N^2)p^2 + (10N^2 - 9)p^4] \\
& - m^4 [150M^8 N^2 + 6M^6 (N^2 + 1)p^2 + M^4 (10N^2 - 3)p^4 + 2M^2 (2N^2 - 3)p^6 + 3p^8] \\
& + m^2 [300M^{10} N^2 + 2M^8 (3 - 149N^2)p^2 + M^6 (4N^2 + 15)p^4 + 9M^4 p^6 - M^2 (4N^2 + 3)p^8 \\
& \left. - (2N^2 + 3)p^{10}] + 150M^8 N^2 Y_1^2 - 2N^2 (M^2 + p^2)^2 (75M^8 + M^6 p^2 + 3M^4 p^4 + 3M^2 p^6 + p^8) \right\} \\
& - \frac{g^2}{128\pi^2 m^4 N p^2} \mathbb{L}_2 (m^2 + 5M^2 N^2) (m^2 - M^2 + p^2), \quad (22)
\end{aligned}$$

and

$$\begin{aligned}
\lambda_3(p^2) = & \frac{g^2 M}{64\pi^2 m^4 N p^4} \left\{ 2 \log\left(\frac{M}{m}\right) [3m^4 (N^2 - 1) (m^2 - M^2) - N^2 p^4 (m^2 - 4M^2) - p^4 m^2 \right. \\
& - p^2 (m^2 - M^2) (m^2 - 3M^2 N^2) - N^2 p^6] - 6m^4 (N^2 - 1) p^2 \\
& - \frac{3\mathbb{L}_1}{Y_1} m^4 (N^2 - 1) [p^2 (m^2 + M^2) + (m^2 - M^2)^2] \\
& \left. - p^2 \mathbb{L}_2 (m^2 - M^2 + p^2) [m^2 + N^2 (p^2 - 3M^2)] \right\}. \quad (23)
\end{aligned}$$

When performing lattice simulations, these functions are obtained from the simulated vertex $\Gamma_\mu(p, -p, 0)$ by projecting in the various tensor structures in the follow-

ing way [24, 25]:

$$\lambda_1(p^2) = \frac{-1}{4g_B} \text{Im} \left(\text{Tr} \gamma_\mu \Gamma_\mu(p, -p, 0) \Big|_{p_\mu=0, p_\nu \neq 0 \text{ for } \mu \neq \nu} \right),$$

$$\lambda_2(p^2) = \frac{1}{4p^2} \sum_{\mu} \left(\frac{1}{4g_B} \text{Im} [\text{Tr} \gamma_{\mu} \Gamma_{\mu}(p, -p, 0)] + \lambda_1(p^2) \right) \quad (24)$$

and

$$\lambda_3(p^2) = \frac{1}{2p^2} \sum_{\mu} p_{\mu} \frac{1}{4g_B} \text{Re} [\text{Tr} \Gamma_{\mu}(p, -p, 0)]$$

where, in these expressions, no implicit sum over repeated indices is meant. It is interesting to note that, in order to extract the function $\lambda_2(p^2)$, a contribution of $\lambda_1(p^2)$ must be added. This issue will be discussed in more detail below.

To compare our results with the lattice simulation of [25] we renormalize the model in the IS scheme and implement the corresponding renormalization group as discussed in Sect. III. It is important to stress that the simulations of [25] have been done in the quenched approximation. Accordingly, we use the beta-functions of the pure Yang-Mills theory derived in [61, 62] for the gluon mass and coupling constant. This implies that the coupling constant and the gluon mass can be fixed once the gluon and ghost 2-point functions have been fitted. The only remaining free parameter is the valence quark mass (and the overall normalization factor). To determine the best fit parameters for the ghost and gluon propagators, we consider the error functions:

$$\begin{aligned} \chi_{AA}^2 &= \frac{1}{4N} \sum_i (\Gamma_{\text{lt.}}^{\perp}(\mu_0)^2 + \Gamma_{\text{lt.}}^{\perp}(p_i)^2) \left(\frac{1}{\Gamma_{\text{lt.}}^{\perp}(p_i)} - \frac{1}{\Gamma_{\text{th.}}^{\perp}(p_i)} \right)^2 \\ \chi_{c\bar{c}}^2 &= \frac{1}{4N} \sum_i (J_{\text{lt.}}^{-2}(\mu_0) + J_{\text{lt.}}^{-2}(p_i)) (J_{\text{lt.}}(p_i) - J_{\text{th.}}(p_i))^2 \end{aligned} \quad (25)$$

We represent these functions in Fig. 2. The best fits are obtained for $g = 4.2$ and mass $m = 0.44$ GeV at the scale 1 GeV which compare well with those found in [61]. As in that reference, this value has been compared to other values of the coupling by taking into account the RG running, finding a good agreement with best estimates up to a 10 % error.

The valence quark mass has been fixed in order to fit properly the quenched quark propagator. More precisely we choose the quark mass in order for the constituent quark mass to match the lattice value. Doing so, one obtains a mass function (the scalar part of the quark propagator, see [64]) that reasonably agree with the lattice data from [73] as can be seen in Fig. 4. One see that this curve mimick the enhancement of the mass in the infrared but not the spontaneous chiral symmetry breaking. Indeed, the constituent quark mass vanishes when the current mass at 1 GeV tends to zero. The corresponding value of the quark mass is $M = 0.2$ GeV at the scale $\mu = 1\text{GeV}$, and it gives a constituent quark mass $M(p = 0) = 0.42$ GeV. These values tend to overestimate the mass function $M(p)$ in the UV by approximately 30% (for example, at 3 GeV we obtain 0.13 GeV

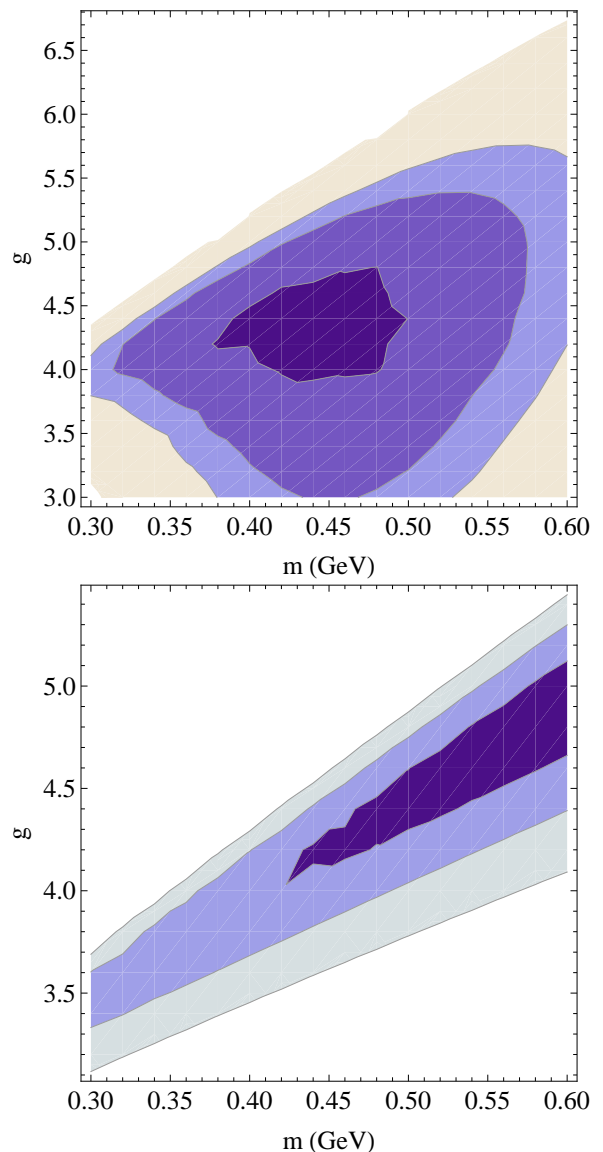


FIG. 2: Contour levels for the error functions χ_{AA} for the gluon propagator (upper panel, for 19%, 22% and 24%) and $\chi_{c\bar{c}}$ for the ghost propagator (lower panel, for 4%, 7% and 10%).

instead of 0.10 GeV) and to underestimate the propagator in the IR (below 1 GeV) by a maximum value of approximately 18%. Having said that, the overall behavior is approximately correct. It must be pointed out when fixing the parameters in order to compare both to the quark mass function and to the vertex functions, a practical difficulty takes place. The simulations have been done for both quantities with different mass parameters. For the quark mass function many bare masses were employed. In the vertex case, the employed values for the bare valence quark mass were $M_0 = 115$ MeV and $M_0 = 60$ MeV [25]. However the authors claim that the vertex functions are almost insensitive to the bare quark mass and employ the data corresponding to

$M_0 = 115$ MeV. In order to have a single set of data we choose the bare valence quark nearest to this value that has been used for propagators which is $M_0 = 75$ MeV. This introduces a systematic error but that do not seem to be large because for relatively small masses like those ⁴, the mass function do not seem to depend on M_0 too much (see [73] and Fig. 4).

One can also analyze the dependence on the valence quark mass of the vertex by studying the error level for the function $\lambda_1(p^2)$ defined as

$$\chi_{\lambda_1}^2 = \frac{1}{N} \sum_i \frac{1}{[\lambda_{1,\text{lt.}}(\mu_0^2)]^2} [\lambda_{1,\text{lt.}}(p_i^2) - \lambda_{1,\text{th.}}(p_i^2)]^2,$$

We also consider the analogous error level for the function $\lambda_3(p^2)$. For this last function the total error may be misleading as discussed below because it average some momenta where the the curve is essentially within error bars with the lowest momenta where errors are much larger. ⁵ They are both shown in Fig. 3. We observe that, even if the optimum value of the masses do not coincide when fitting $\lambda_1(p^2)$ and $\lambda_3(p^2)$, there is a region of parameters where both errors are reasonably small (that is less than 10%). Moreover, the value of the gluon mass extracted from the ghost and gluon propagators ($m = 0.44$ GeV) is within an error region with less than 20%. It is important to stress that once the parameters g , m and M have been fixed, they are used for the calculation of the quark-gluon vertex for all momentum configurations. Accordingly, they become pure predictions without free parameters of the present calculation.

The resulting curves for the functions $\lambda_1(p^2)$, $\lambda_2(p^2)$ and $\lambda_3(p^2)$ can be seen in Fig. 5. We find a good agreement for the function $\lambda_1(p^2)$. All the point are below a 16% of error except the first point ($p = 140$ MeV) where a larger error is observed (27%). Let us point out, however that our curve is systematically below the lattice one. The behavior for $\lambda_3(p^2)$ is qualitatively reproduced, with a strong increase (in absolute value) at momenta of the order of 1 GeV This last curve depends more strongly on the quark mass. This can be understood by the observation that λ_3 tends to zero in the chiral limit, see Table I. The function is very well reproduced (essentially within error bars) except for the two lowest momenta ($p = 140$ and 400 MeV) where the errors are larger (37% and 33% respectively when comparing to the lattice central value). Let us, however, point out that the statistical error bars of these lattice points are large (22% in both points).

⁴ These values for the mass are not small with respect to actual physical values of the masses for light quarks. However, they are relatively small with respect to typical QCD scales and, in consequence, some quantities are not very sensitive to them.

⁵ As discussed in detail below, the comparison of our results with lattice simulations for the function $\lambda_2(p^2)$ is problematic. Consequently, we do not use this function for fitting the parameters.

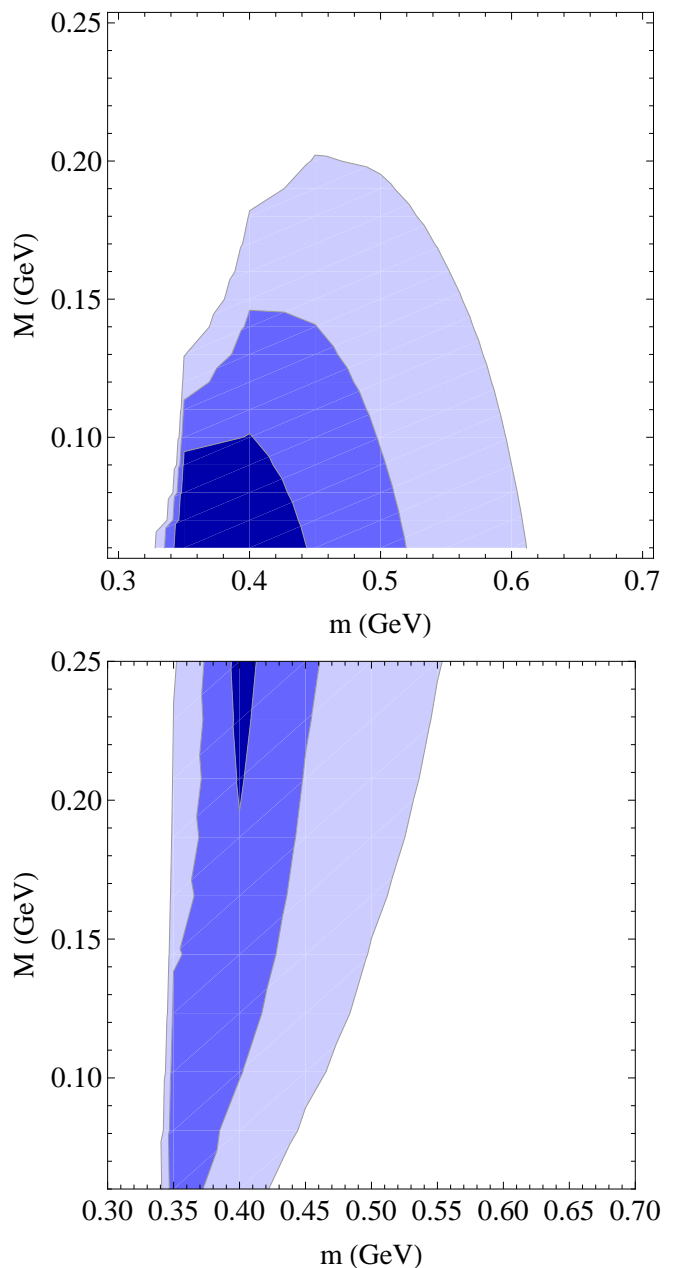


FIG. 3: Contour levels for the quantity χ_{λ_1} (upper panel) and χ_{λ_3} (lower panel) in the plane of gluon mass vs. quark mass. The contour lines correspond to 4%, 4.5% and 5% for χ_{λ_1} and 10%, 20% and 30% for χ_{λ_3} .

We therefore find that for a unique choice of parameters g , m and M , we reproduce very well the ghost and gluon propagators and reasonably well the mass function $M(p)$ and the vertex functions λ_1 and λ_3 , which is a highly nontrivial result.

The situation looks qualitatively different for the function $\lambda_2(p^2)$, which tends to a constant at zero momentum in our approach while it diverges in the lattice data. This disagreement was already observed in previous analytical treatments of this function [21, 22] and was interpreted

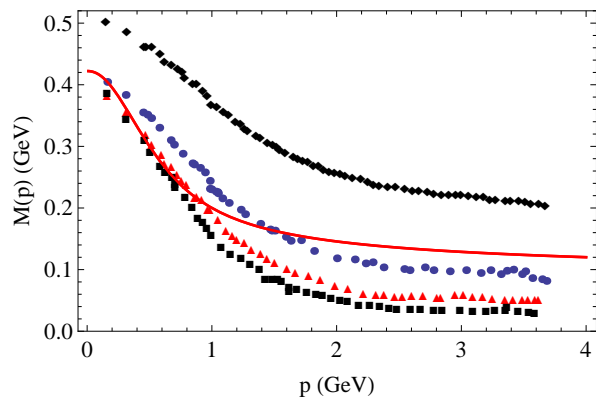


FIG. 4: Quark mass as a function of the momentum. The renormalization group flow is initialized at 1 GeV with $g = 4.2$, $m = 0.44$ GeV, and $M = 0.2$ GeV. Lattice data [73] are marked with dots and parametrized by their bare masses: $M_0 = 19$ MeV (squares), $M_0 = 37$ MeV (triangles), $M_0 = 75$ MeV (circles), $M_0 = 187$ MeV (diamond).

as a consequence of the non-perturbative features of the theory. We want to propose a completely different explanation for this phenomenon. Let us go back to Eq. (24) which is used to extract λ_2 from the lattice data. We observe that we must subtract from the function $\lambda_1(p^2)$ a quantity

$$\tilde{\lambda}_2 = -\frac{1}{16g_B} \sum_{\mu} \text{Im Tr} [\gamma_{\mu} \Gamma_{\mu}(p, -p, 0)]. \quad (26)$$

which is directly extracted from lattice data. The difference is then divided by p^2 . In our calculation, the fact that λ_2 tends to a constant originates from a compensation of these two terms in the limit $p \rightarrow 0$, the difference being of order p^2 . We can interpret this constant as a compensation of large numbers, a situation which is difficult to treat numerically. Indeed, a small error in one of these two terms would lead to a divergence of $\lambda_2(p^2)$ when $p \rightarrow 0$ but this would be certainly an artifact.

Note that such a divergence in $\lambda_2(p^2)$ would imply a nonanalytic behavior of the vertex function at small momenta [see Eq. (20)] since the $p \rightarrow 0$ limit would depend on the direction (in momentum space) which is used to perform this limit. In our calculations, which are done in the framework of the action (1)–(2), the only non-analytic behaviors observed so far are a consequence of ghost loops (see, for example, [61–63]). Such contributions are not present at one-loop order in the present vertex and most probably their contributions of higher order should be extremely small.

If the disagreement takes its origin in partial compensations in the extraction of the $\lambda_2(p^2)$ function from the formula (24), the comparison should be better for the quantity that is directly extracted from lattice data (that is $\tilde{\lambda}_2$) than that for λ_2 itself. In Fig. 6 we compare our prediction for $\tilde{\lambda}_2$ to the corresponding lattice values. We observe a very good agreement in both expressions: our

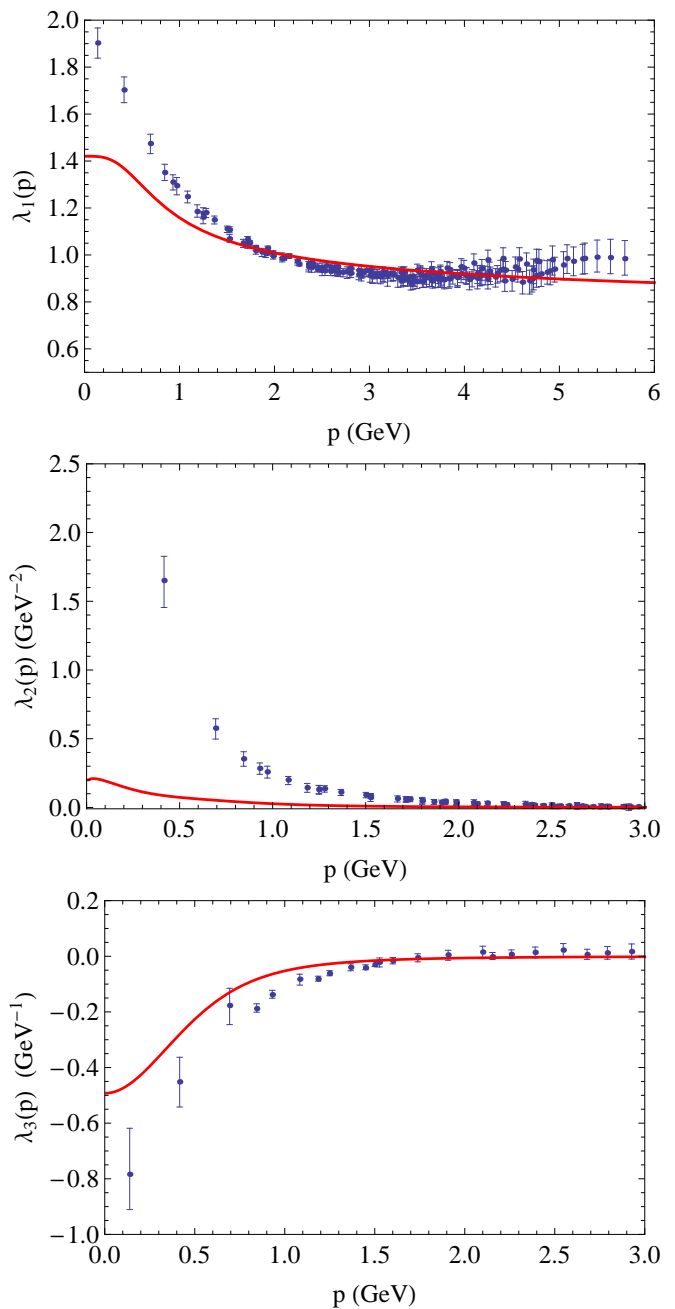


FIG. 5: Scalar functions of the quark-gluon vertex: λ_1 (top), λ_2 (middle) and λ_3 (bottom) for a vanishing gluon momentum, as a function of the quark momentum. The line are the one-loop results with $M = 0.2$ GeV. The dots correspond to the lattice data of [25].

curve is almost within the lattice error bars except for the lowest momentum where the error is around the 17% with respect to the central value of simulations. We must, however point out that the curve is systematically above the central values of lattice data. The agreement between the $\tilde{\lambda}_2$ with lattice data suggests that the true origin of the disagreement between analytical and lattice data for λ_2 lies in the difficulty of obtaining a function from differ-

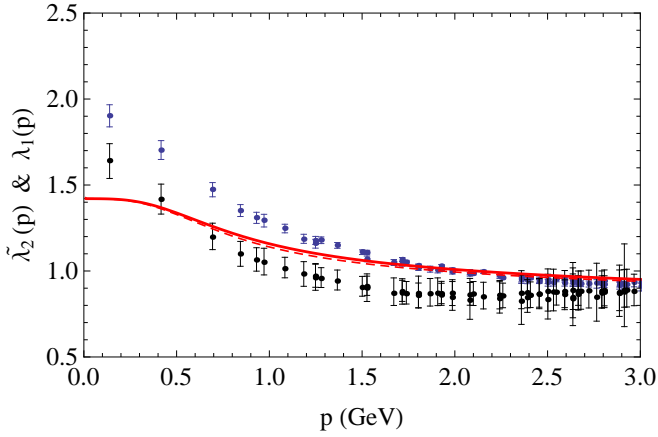


FIG. 6: Comparison of the quantities λ_1 and $\tilde{\lambda}_2$ as a function of the momentum [see Eq. 26]. Our one-loop results for λ_1 (full line) are almost degenerate with those for $\tilde{\lambda}_2$ (dashed line). The higher (blue) points correspond to λ_1 and the lower (grey) ones to $\tilde{\lambda}_2$, extracted from [25]. In the latter case, our estimation of the error bar is probably pessimistic.

ences of large numbers. Let us point out that the origin of the error is certainly not statistical. If it were so, the signal obtained from the lattice data for $\lambda_2(p^2)$ would be extremely noisy. Most probably the origin of the error is more systematical. Now it is important to recall that the lattice extraction of these scalar function requires a careful treatment of various lattice artifacts (see [24, 25]). A mismatch in the treatment of lattice artifact of the longitudinal and transverse parts of the vertex could easily introduce a systematic error that, when divided by p^2 , gives a large spurious contribution in the estimate of $\lambda_2(p^2)$. In any case, Fig. 6 shows clearly that not only the component transverse to the external momentum but also the longitudinal one are correctly reproduced by the present one-loop calculation.

B. Quark and anti-quark with equal momenta

In this section we present the results for the kinematic configuration given by equal momenta of quark and anti-quark ($r = p$) and, accordingly, $k = -2p$. In this kinematics the quark-gluon vertex simplifies considerably

$$\Gamma_\mu(p, p, -2p) = -ig [\lambda_1(p^2)\gamma_\mu + 4\tau_3(p^2)(\not{p}p_\mu - p^2\gamma_\mu) - 2i\tau_5(p^2)\sigma_{\mu\nu}p_\nu]$$

and the transverse projected vertex (that is $P_{\mu\nu}^\perp(p)\Gamma_\nu(p, p, -2p)$) has the form

$$\Gamma_\mu^P(p, p, -2p) = -ig \left[\lambda'_1(p^2) \left(\gamma_\mu - \frac{\not{p}p_\mu}{p^2} \right) - 2i\tau_5(p^2)\sigma_{\mu\nu}p_\nu \right]$$

where we have introduced $\lambda'_1 = \lambda_1 - k^2\tau_3$.

In spite of this simplification, for this configuration of momenta, integrals can not be done analytically and

some remaining Feynman parameter integrals must be performed numerically. Fortunately, having fixed the parameters from propagators, the calculation must be done only once for a given choice of parameters.

In this kinematic configuration, the scalar functions λ'_1 and τ_5 are extracted from the vertex as

$$\lambda'_1 = -\frac{1}{3} \sum_\mu \frac{1}{4g_B} \text{Im} (\text{Tr} \gamma_\mu \Gamma_\mu^P(p, p, -2p))$$

and

$$\tau_5 = \frac{1}{3k^2} \sum_{\mu,\nu} k_\mu \frac{1}{4g_B} \text{Re} (\text{Tr} \sigma_{\mu\nu} \Gamma_\mu^P(p, p, -2p)).$$

In this case, no subtraction is needed to extract λ'_1 and τ_5 from the lattice data.

In Fig. 7 we compare our one-loop results with the lattice data using the same initial condition of the coupling constant and masses as in the previous case, $g = 4.2$, $m = 0.44$ GeV and for the value of $M = 0.2$ GeV at $\mu_0 = 1$ GeV. We observe that the function λ'_1 is well reproduced by our results (mostly within the lattice error bars, except for the lowest momentum point where the error is of the order of 25%). The other function τ_5 is seen to be very sensitive to the choice of the quark mass at 1 GeV. Again, this is a consequence of the fact that, in the chiral limit, this function tends to zero, see Table I. We observe that the qualitative behavior for this function is reproduced but the agreement is not quantitative. In particular, our one-loop results do not reach such large values in the deep infrared where for the lowest value of momenta the error reach 45%. Moreover, the curve is systematically above the lattice curve. This is similar to what has already been observed in the DS results of [22].

C. Symmetric configuration

In this subsection we consider the case where the quark and antiquark have momenta with the same modulus but can have arbitrary angle between them (or, equivalently, that one can vary the value of the gluon momentum). It is clear that the two previous kinematic configurations correspond to particular cases of the more general situation considered here. However, more general configurations of momenta were studied in the lattice [26], but only for a particular tensorial structure. More precisely, in terms of the tensorial decomposition (5), the function that is extracted in the lattice is $\lambda'_1 = \lambda_1 - k^2\tau_3$ as in the previous case. We limit to three particular kinematic configurations. In the first two, the modulus of the gluon momentum taking values $|k| = 0.277$ GeV and $|k| = 0.838$ GeV. The third corresponds to the completely symmetric case where the modulus of the three momenta are equal $r^2 = p^2 = k^2$. As before, initial conditions of the renormalization group equations correspond again to $g = 4.2$, $m = 0.44$ GeV and $M = 0.2$ GeV at $\mu_0 = 1$ GeV.

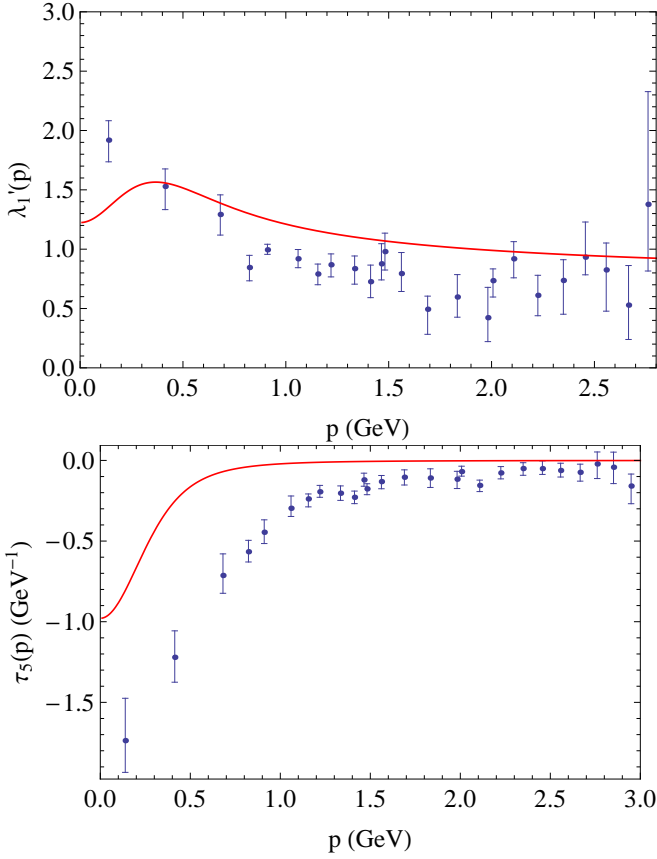


FIG. 7: Scalar function of the quark-gluon vertex: λ'_1 (top) and τ_5 (bottom) for equal momentum (p) for the quark and antiquark. The full line are the one-loop results and the dots correspond to the lattice data of [25].

The results are presented in Figs. 8 and 9. For $|k| = 0.277$ GeV the maximal error is of 12%. For $|k| = 0.838$ GeV, our results are within lattice error bars with the exception of the point of lowest momentum ($p = 0.4$ GeV) where the error is of 18%. In the completely symmetric configuration the curve is almost within error bars except for the lowest momentum where the error is 25%. At the end of this section we discuss on possible origins of these discrepancies.

D. Unquenched vertex

We conclude our study by introducing the effect of dynamic quarks in our calculations. This influences the renormalization factor for the gluon Z_A and for the gluon mass Z_{m^2} , which both have a contribution from a fermion closed loop. On the contrary, the first contribution of dynamic quarks to Z_c and to the quark-gluon vertex comes at two loops. We conclude that the effect of dynamic quarks only influence indirectly our calculation, through the modification of the β functions for the coupling constant and the gluon mass and for the field renormalization

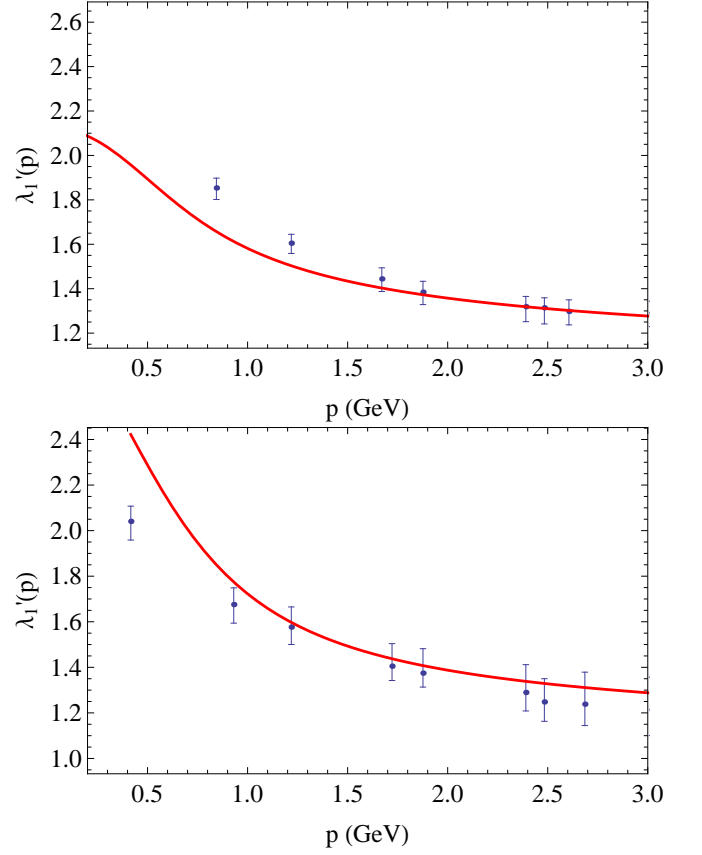


FIG. 8: Scalar function of the quark-gluon vertex $\lambda'_1 = \lambda_1 - k^2 \tau_3$ for $r^2 = p^2$ and $k = 0.277$ GeV (top) and $k = 0.838$ GeV (bottom). The full line are the one loop results and the dots the lattice data of [70].

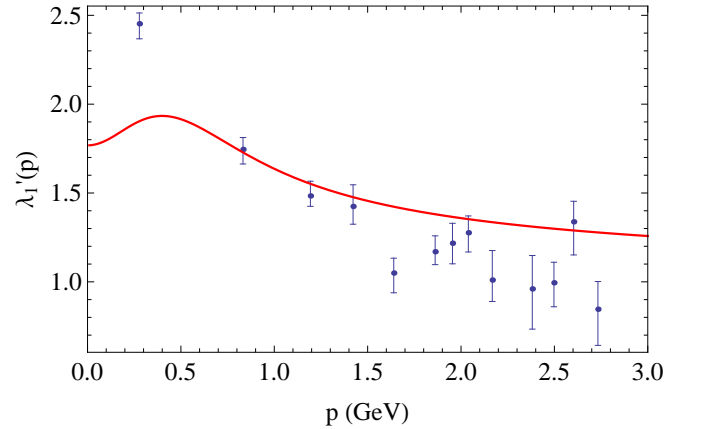


FIG. 9: Scalar function of the quark-gluon vertex $\lambda'_1 = \lambda_1 - k^2 \tau_3$ for the completely symmetric configuration $r^2 = p^2 = k^2$. The full line are the one loop results and the dots the lattice data of [70] interpolated to reconstruct the symmetric configuration.

z_A .

The unquenched propagators for the quarks, gluons and ghosts were studied in [64], in the framework of the Curci-Ferrari action. We use here the parameters that were obtained in that article, as best fits when comparing with the lattice data in the only case where the mass quark can be fixed from the a quark mass function, that is $N_f = 2+1$. The best fit parameters in this case is $g = 4.8$, $m = 0.42$ GeV and $M = 0.08$ GeV at $\mu_0 = 1$ GeV. The corresponding values of the couplings were compared in [64] with standard estimates of the coupling giving an agreement with an error of the order of 17 %, which is similar to the typical overall error in the infrared of the one-loop approximation.

Using these values of the parameter we can now predict the vertex in the unquenched case. It is interesting to note that in the present procedure this is an extremely simple calculation once the beta functions have been calculated and the parameters fixed by comparing to the 2-point functions. This is in contrast to lattice simulations that are extremely costly in the unquenched case. This is probably the reason why there are, to our knowledge, no lattice data for this vertex.

We focus here on the zero gluon momentum but other tensorial structures and kinematic configuration could be presented as well. We present in Fig. 10 the three scalar functions λ_1 , $\tilde{\lambda}_2$ and λ_3 for different number of flavors. The presence of dynamic quarks clearly tends to increase these functions at low energy.

E. Possible origin of discrepancies

The overall agreement of the present one-loop calculation is reasonably good. Most of the lattice data are well reproduced with a good accuracy. It is important to stress that most of the calculations are pure predictions without free parameters (that are already adjusted via 2-point functions) and that they are all obtained by one loop calculations.

However, some discrepancies are present and we analyze them in the present subsection. Putting aside the $\lambda_2(p)$, the largest discrepancy concerns the $\tau_5(p)$ function in the equal momenta configuration. Even if in this case the order of magnitude of the function and general behavior is well reproduced, there is not quantitative agreement. Finally, one observes some quantitative disagreement for the function $\lambda'_1(p)$ function in the symmetric configuration at small momenta. We can say that there is a good general agreement with lattice data but the quantitative agreement is not as good as for gluon and ghost vertices. A similar behavior is observed in the study of propagators [64].

We give now two possible (probably complementary) explanations for this. First, one of the reasons of the success of a perturbative analysis in the gluon and ghost sector is that the relevant couplings (the value of the 3-gluon and ghost-gluon couplings) are moderate except, for the

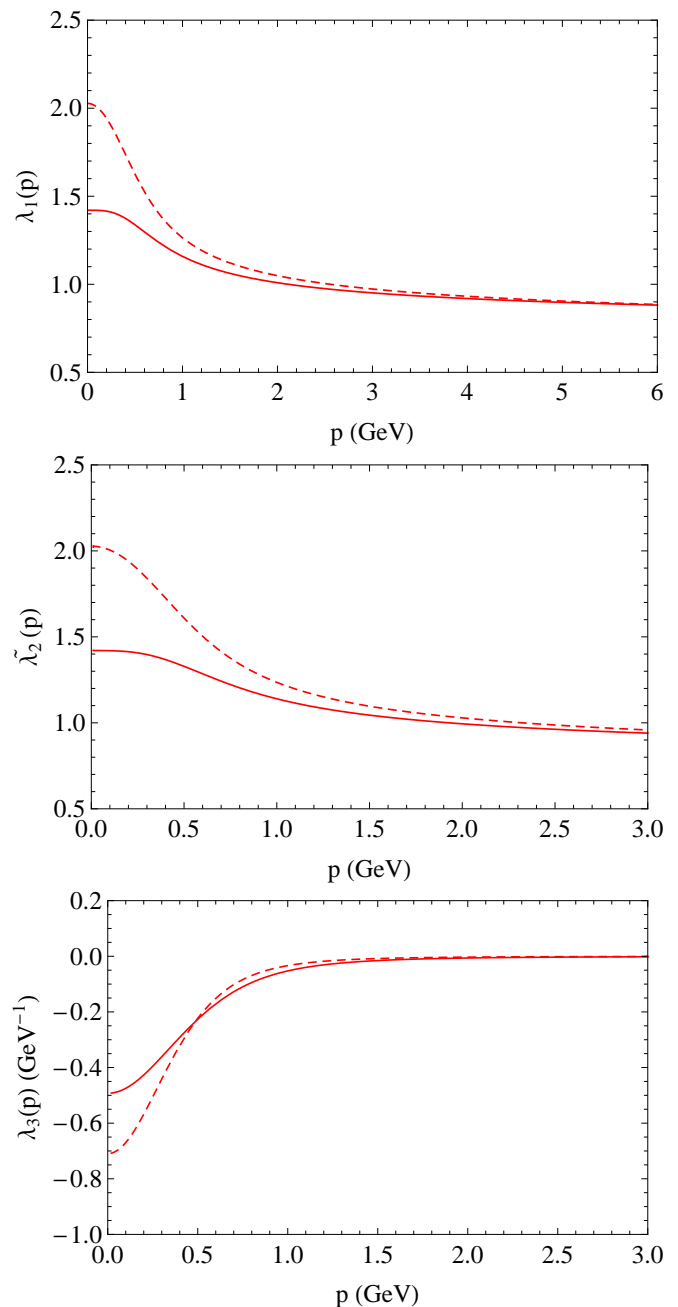


FIG. 10: Scalar functions of the quark-gluon vertex in the unquenched case. λ_1 (top), $\tilde{\lambda}_2$ (middle) and λ_3 (bottom) for a vanishing gluon momentum, as a function of the quark momentum. The curves corresponds to For $N_f = 0$ (full line) and $N_f = 2+1$ (small dashes).

3-gluon vertex for very small values of the coupling where the presence of the gluon mass, has already suppressed fluctuations. However, in the quark sector, even if the coupling does not presents a Landau pole, it reaches significantly larger values than in the pure-gluon sector. One measure of this is the value of the coupling $\lambda_1(p)$ or $\lambda'_1(p)$. One can define a natural running coupling function for this functions as $\alpha_s^{\text{quark-gluon}}(p) = (\lambda'_1(p))^2 \alpha_s^{\text{ghost-gluon}}(p)$.

It is important to stress that even if for $p \gg m$, all the definitions of the running coupling give a universal beta function, this is not the case for momenta $p \lesssim m$. In consequence, the moderate values of the coupling in a certain scheme does not exclude that it may be large in some other scheme. In particular, one observes that for small values of p the quark-gluon coupling is larger by a factor of 2.4 with respect to the ghost-gluon coupling (giving a larger expansion parameter by a factor $(2.4)^2 \simeq 5.8$). In a sense, this is to be expected because it is well established (see, for example, [3]) that the quark-gluon coupling that is required for generating Dynamical Chiral Symmetry Breaking (DSCB) is larger than the one that is extracted from the ghost-gluon vertex. Now, the expansion parameter of the perturbative expansion in the present model in the ghost-gluon sector (precisely discussed in [61]) may reach values of the order of 0.2. In consequence, the expansion parameter in the quark-gluon sector seem to put the perturbative expansion in trouble at very low momenta. This may indicate that even in the present model where the ghost-gluon sector seem to be treatable perturbatively, some sort of partial resummation is needed in the quark sector (or, at least, in part of it). These facts also reflect on a certain tension when the parameters have to be chosen in order to fit all the data at the same time. Even if the overall agreement is good with a single set of parameters, a precise renormalization scheme had to be chosen because at very low momenta an important sensitivity is observed.

This last point is related to a second possible origin of discrepancies. In the quark-gluon vertex, the quantities that are not sensitive to the DCSB are much better estimated than those that are sensitive to it. The function $\lambda_1(p)$, gives better agreement than the $\lambda_3(p)$ or the $\tau_5(p)$ (which are sensitive to the DSBC). This manifests also in the fact that those quantities seem to have a larger sensitivity on the renormalization conditions. Now, it is not clear in what measure we have properly taken into account the role of the DSBC. Even if RG effect gives an important enhancement of the quark mass in the infrared that quantitatively reasonably reproduces the mass function measured in the lattice, it is unclear at the moment if a proper treatment DSBC will require to use more sophisticated techniques as the introduction of composite fields for the chiral condensate. This may be at the origin of the lower quality of quantities that are sensitive to the DSBC.

V. CONCLUSION

In this article, we have presented the calculation of the quark-gluon vertex at one loop in the massive (Curci-Ferrari) extension of the Landau gauge. The results were decomposed on the twelve independent tensorial structures. We implement the renormalization-group improvement so as to avoid large logarithms. We find that these analytic results compare qualitatively well with the quenched lattice data. In one case (λ_2 for a vanishing gluon mass), the difference between lattice data (that predicts a divergence at low momentum) and our (which are finite at small momenta) may be attributed to a difference of large numbers when extracting this function from lattice data.

At the quantitative level, we observe that the quantities that are not forbidden by chiral symmetry are reproduced at the level of 10% except for momenta of the order of 100-200 MeV where larger errors are found, as detailed in the results section. The others are much more difficult to reproduce and show strong dependence on the renormalization-group scheme. This is probably to be attributed to the rather crude treatment of chiral symmetry breaking in our calculation. Moreover, in order to fit simultaneously both the mass function coming from the quark propagator and the vertex function, a certain tension in the choice of parameters is observed and in order for this to be fulfilled it is necessary to choose a precise renormalization scheme. It is interesting to point out that even if, at the end, the agreement of the present one-loop calculation is reasonably good, the precision is not as good as in the ghost-gluon sector. This may be related to a larger value of the associated coupling and some sort of resummation in this sector could be useful. This issues will be addressed in the future.

Acknowledgments

We thank J.-I. Skullerud for kindly making available the lattice data and for useful exchanges. We acknowledge partial support from PEDECIBA and ECOS-Sud (U11E01) programs.

-
- [1] C. S. Fischer and R. Alkofer, Phys. Rev. D **67**, 094020 (2003).
 - [2] M. S. Bhagwat, A. Holl, A. Krassnigg, C. D. Roberts and P. C. Tandy, Phys. Rev. C **70**, 035205 (2004).
 - [3] R. Alkofer, C. S. Fischer, F. J. Llanes-Estrada and K. Schwenzer, Annals Phys. **324**, 106 (2009).
 - [4] H. H. Matevosyan, A. W. Thomas and P. C. Tandy, Phys. Rev. C **75** (2007) 045201.
 - [5] V. A. Karmanov and P. Maris, Few Body Syst. **46**, 95 (2009) [arXiv:0811.1100 [hep-ph]].
 - [6] A. Krassnigg, Phys. Rev. D **80**, 114010 (2009) [arXiv:0909.4016 [hep-ph]].
 - [7] D. Nicmorus, G. Eichmann and R. Alkofer, Phys. Rev. D **82**, 114017 (2010) [arXiv:1008.3184 [hep-ph]].
 - [8] H. L. L. Roberts, L. Chang, I. C. Cloet and C. D. Roberts, Few Body Syst. **51**, 1 (2011)

- [arXiv:1101.4244 [nucl-th]].
- [9] H. Sanchis-Alepuz, R. Williams and R. Alkofer, Phys. Rev. D **87**, no. 9, 096015 (2013) [arXiv:1302.6048 [hep-ph]].
- [10] C. S. Fischer, S. Kubrak and R. Williams, Eur. Phys. J. A **50**, 126 (2014) [arXiv:1406.4370 [hep-ph]].
- [11] J. S. Ball and T. W. Chiu, Phys. Rev. D **22**, 2542 (1980).
- [12] A. I. Davydychev, P. Osland and L. Saks, Phys. Rev. D **63**, 014022 (2001).
- [13] J. A. Gracey, Phys. Rev. D **90**, 025014 (2014).
- [14] G. Curci and R. Ferrari, Nuovo Cim. A **32**, 151 (1976).
- [15] F. Delduc and S. P. Sorella, Phys. Lett. B **231**, 408 (1989).
- [16] M. Tissier and N. Wschebor, Phys. Rev. D **79**, 065008 (2009).
- [17] J. C. Taylor, Nucl. Phys. B **33** (1971) 436.
- [18] D. Dudal, H. Verschelde and S. P. Sorella, Phys. Lett. B **555**, 126 (2003).
- [19] N. Wschebor, Int. J. Mod. Phys. A **23**, 2961 (2008).
- [20] J. A. Gracey, Phys. Lett. B **552**, 101 (2003).
- [21] R. Williams, arXiv:1404.2545 [hep-ph].
- [22] A. C. Aguilar, D. Binosi, D. Ibañez and J. Papavassiliou, Phys. Rev. D **90**, no. 6, 065027 (2014).
- [23] M. Mitter, J. M. Pawłowski and N. Strodthoff, Phys. Rev. D **91**, 054035 (2015) [arXiv:1411.7978 [hep-ph]].
- [24] J. Skullerud and A. Kizilersu, JHEP **0209**, 013 (2002).
- [25] J. I. Skullerud, P. O. Bowman, A. Kizilersu, D. B. Leinweber and A. G. Williams, JHEP **0304**, 047 (2003).
- [26] A. Kizilersu, D. B. Leinweber, J. I. Skullerud and A. G. Williams, Eur. Phys. J. C **50**, 871 (2007).
- [27] P. Boucaud, G. Burgio, F. Di Renzo, J. P. Leroy, J. Micheli, C. Parrinello, O. Pene and C. Pittori *et al.*, JHEP **0004**, 006 (2000).
- [28] V. N. Gribov, Nucl. Phys. B **139** (1978) 1.
- [29] D. Zwanziger, Nucl. Phys. B **323**, 513 (1989).
- [30] D. Zwanziger, Nucl. Phys. B **399**, 477 (1993).
- [31] D. Zwanziger, Phys. Rev. D **65**, 094039 (2002).
- [32] D. Dudal, J. A. Gracey, S. P. Sorella, N. Vandersickel and H. Verschelde, Phys. Rev. D **78**, 125012 (2008).
- [33] P. van Baal, Nucl. Phys. B **369**, 259 (1992).
- [34] L. von Smekal, R. Alkofer and A. Hauck, Phys. Rev. Lett. **79**, 3591 (1997).
- [35] R. Alkofer and L. von Smekal, Phys. Rept. **353**, 281 (2001).
- [36] J. C. R. Bloch, Few Body Syst. **33** (2003) 111.
- [37] C. S. Fischer and H. Gies, JHEP **0410**, 048 (2004) [hep-ph/0408089].
- [38] C. S. Fischer, A. Maas and J. M. Pawłowski, Annals Phys. **324** (2009) 2408.
- [39] J. Berges, N. Tetradis and C. Wetterich, Phys. Rept. **363**, 223 (2002) [hep-ph/0005122].
- [40] A. Sternbeck, L. von Smekal, D. B. Leinweber and A. G. Williams, PoS LAT **2007**, 340 (2007).
- [41] A. Cucchieri and T. Mendes, Phys. Rev. Lett. **100**, 241601 (2008).
- [42] A. Cucchieri and T. Mendes, Phys. Rev. D **78**, 094503 (2008).
- [43] A. Sternbeck and L. von Smekal, Eur. Phys. J. C **68**, 487 (2010).
- [44] A. Cucchieri and T. Mendes, Phys. Rev. D **81**, 016005 (2010).
- [45] I. L. Bogolubsky, E. M. Ilgenfritz, M. Muller-Preussker and A. Sternbeck, Phys. Lett. B **676**, 69 (2009).
- [46] D. Dudal, O. Oliveira and N. Vandersickel, Phys. Rev. D **81**, 074505 (2010).
- [47] P. O. Bowman, U. M. Heller, D. B. Leinweber, M. B. Parappilly and A. G. Williams, Phys. Rev. D **70**, 034509 (2004).
- [48] M. B. Parappilly, P. O. Bowman, U. M. Heller, D. B. Leinweber, A. G. Williams and J. B. Zhang, AIP Conf. Proc. **842**, 237 (2006).
- [49] A. C. Aguilar and A. A. Natale, JHEP **0408**, 057 (2004).
- [50] Ph. Boucaud *et al.*, JHEP **06** (2006) 001.
- [51] A. C. Aguilar and J. Papavassiliou, Eur. Phys. J. A **35** (2008) 189.
- [52] A. C. Aguilar, D. Binosi and J. Papavassiliou, Phys. Rev. D **78** (2008) 025010.
- [53] P. Boucaud, J. P. Leroy, A. Le Yaouanc, J. Micheli, O. Pene and J. Rodriguez-Quintero, JHEP **06** (2008) 099.
- [54] J. Rodriguez-Quintero, JHEP **1101** (2011) 105.
- [55] M. Q. Huber and L. von Smekal, JHEP **04**, 149 (2013).
- [56] C. Becchi, A. Rouet and R. Stora, Commun. Math. Phys. **42**, 127 (1975).
- [57] C. Becchi, A. Rouet and R. Stora, Annals Phys. **98**, 287 (1976).
- [58] I. V. Tyutin, arXiv:0812.0580 [hep-th].
- [59] A. Cucchieri, T. Mendes and A. R. Taurines, Phys. Rev. D **71**, 051902 (2005) [hep-lat/0406020].
- [60] P. O. Bowman, U. M. Heller, D. B. Leinweber, M. B. Parappilly, A. Sternbeck, L. von Smekal, A. G. Williams and J. b. Zhang, Phys. Rev. D **76**, 094505 (2007) [hep-lat/0703022 [HEP-LAT]].
- [61] M. Tissier and N. Wschebor, Phys. Rev. D **84** (2011) 045018.
- [62] M. Tissier and N. Wschebor, Phys. Rev. D **82** (2010) 101701.
- [63] M. Peláez, M. Tissier and N. Wschebor, Phys. Rev. D **88** (2013) 125003.
- [64] M. Peláez, M. Tissier and N. Wschebor, Phys. Rev. D **90** (2014) 6, 065031.
- [65] U. Reinosa, J. Serreau, M. Tissier and N. Wschebor, Phys. Lett. B **742** (2015) 61.
- [66] U. Reinosa, J. Serreau, M. Tissier and N. Wschebor, Phys. Rev. D **91** (2015) 4, 045035.
- [67] U. Reinosa, J. Serreau and M. Tissier, arXiv:1504.02916 [hep-th].
- [68] G. Passarino and M. J. G. Veltman, Nucl. Phys. B **160** (1979) 151.
- [69] Supplemental material where the different scalar functions are expressed in terms of the Passarino-Veltman integral.
- [70] J. I. Skullerud, P. O. Bowman, A. Kizilersu, D. B. Leinweber and A. G. Williams, Nucl. Phys. Proc. Suppl. **141**, 244 (2005).
- [71] A. Sternbeck, K. Maltman, M. Muller-Preussker and L. von Smekal, PoS LATTICE **2012** (2012) 243.
- [72] A. Ayala, A. Bashir, D. Binosi, M. Cristoforetti and J. Rodriguez-Quintero, Phys. Rev. D **86** (2012) 074512.
- [73] P. O. Bowman, U. M. Heller, D. B. Leinweber, M. B. Parappilly, A. G. Williams and J. b. Zhang, Phys. Rev. D **71** (2005) 054507.